Statistical Distribution of Bifurcation of Earth's Inner Energetic

2	Electron Belt at tens of keV
3	Man Hua ¹ , Binbin Ni ^{1,2} , Wen Li ³ , Qianli Ma ^{3, 4} , Xudong Gu ¹ , Song Fu ¹ , Xing Cao ¹ ,
4	Yingjie Guo ¹ , and Yangxizi Liu ¹
5	¹ Department of Space Physics, School of Electronic Information, Wuhan University, Wuhan,
6	Hubei 430072, China.
7	² CAS Center for Excellence in Comparative Planetology, Hefei, Anhui, China.
8	³ Center for Space Physics, Boston University, Boston, Massachusetts, USA.
9	⁴ Department of Atmospheric and Oceanic Sciences, UCLA, Los Angeles, California, USA.
10	
11	Corresponding author: Prof. Binbin Ni, Wuhan University, Email: bbni@whu.edu.cn
12	
13	Key Points
14	· Statistics of bifurcated inner energetic electron belt is investigated using 6-year Van Allen
15	Probes measurements
16	• The bifurcated inner belt is mostly observed at \sim 30-100 keV with the bifurcation dip at L
17	~2.0 - 2.3 under quiet geomagnetic conditions
18	· Energy and seasonal dependences of the inner belt bifurcation support the important role of
19	VLF transmitter signals in its formation
20	
21	Abstract
22	We present a survey of the bifurcation of the Earth's energetic electron belt (tens of keV) using
23	6-year measurements from Van Allen Probes. The inner energetic electron belt usually presents
24	one-peak radial structure with high flux intensity at $L < \sim 2.5$, which however can be bifurcated to
25	exhibit a double-peak radial structure. By automatically identifying the events of bifurcation
26	based on RBSPICE data, we find that the bifurcation is mostly observed at ~30-100 keV with a
27	local flux minimum at $L=\sim2.0-\sim2.3$ under relatively quiet geomagnetic conditions, typically
28	after a significant flux enhancement due to radial diffusion or injections to $L < 2.5$. The
29	bifurcation typically lasts for a few days during quiet periods until interrupted by injections or
30	radial diffusion. The L-shell, energy and seasonal dependences of the occurrence of bifurcated

inner electron belt support the important role of electron scattering by very-low-frequency transmitter waves in the bifurcation formation.

Plain Language Summary

The Earth's inner energetic electron belt typically exhibits one-peak radial structure with high flux intensities at radial distances < \sim 2.5 Earth radii. Recent studies suggested that human-made very-low-frequency (VLF) transmitters leaked into the inner magnetosphere can efficiently scatter energetic electrons, bifurcating the inner electron belt. In this letter, we use 6-year electron flux data from Van Allen Probes to comprehensively analyze the statistical distributions of the bifurcated inner electron belt and their dependence on electron energy, season, and geomagnetic activity, which is crucial to understand when and where VLF transmitters can efficiently scatter electrons in addition to other naturally occurring waves. We reveal that bifurcation can be frequently observed for tens of keV electrons under relatively quiet geomagnetic conditions, typically after significant flux enhancements that elevate fluxes at $L = 2.0 - \sim 2.5$ providing the prerequisite for the bifurcation. The bifurcation typically lasts for a few days until interrupted by substorm injections or inward radial diffusion. The L-shells of bifurcation dip decrease with increasing electron energy, and the occurrence of bifurcation is higher during northern hemisphere winter than summer, supporting the important role of VLF transmitter waves in energetic electron loss in near-Earth space.

Key words: Inner electron radiation belt; Flux bifurcation; VLF transmitter waves;

Statistical distribution

1. Introduction

The Earth's inner electron radiation belt, which typically exhibits one-peak structure with high flux intensities at L-shells below ~2.5 (e.g., Reeves et al., 2016), can manifest various acceleration and loss processes for energetic electrons above tens of keV (e.g., Baker et al., 2004, 2007; Baker & Blake, 2012; Claudepierre et al., 2020a). Electron flux can exhibit sudden enhancement or injection features during geomagnetic active times (e.g., Claudepierre et al., 2019; Hua et al., 2019) followed by a long period of decay (e.g., Rosen & sanders, 1971; Gu et

62 al., 2020; Ma et al., 2020). Inner belt electron lifetimes are mainly controlled by Coulomb 63 collision (Walt & Farley, 1978) and cosmic ray albedo neutron decay (Xiang et al., 2019, 2020) 64 at very low L-shells close to the inner edge of the inner belt, while at higher L-shells waveparticle interactions due to very-low-frequency (VLF) transmitter waves, lightning-generated 65 66 whistlers, and plasmaspheric hiss play a more important role in driving energy-dependent pitch-67 angle scattering, which can further lead to electron loss (e.g., Abel and Thorne, 1998a, 1998b; 68 Albert et al., 2016; Cao et al., 2017, 2020; Claudepierre et al., 2020b; Green et al., 2020; Ma et 69 al., 2016; Meredith et al., 2007; Ni et al., 2014, 2019; Rodger and Clilverd, 2002; Rodger et al., 70 2003; Zhang et al., 2019; Zhao et al., 2019).

71

72

73

74

75

76

77

78

79

80

81

82

83

84

85

86

87

88

89

90

91

92

Narrow-band electromagnetic waves originated from ground-based VLF transmitter signals with a typical frequency range of 18–27 kHz can propagate in the whistler mode, whose wave amplitude tends to peak at nightside within $L < \sim 3$ (Chen et al., 2016, 2017; Clilverd et al., 2008; Ma et al., 2017; Meredith et al., 2019, Yi et al., 2019). The NWC transmitter located in Australia (19.8 kHz, L = 1.42, 1000 kW) and the NAA transmitter located in North America (24.0 kHz, L = 2.74, 1000 kW) are the two most powerful stations (Meredith et al., 2019). DEMETER satellite observations have indicated strong correlations between electron flux enhancements in the drift-loss cone and VLF transmitters locations (Gamble et al., 2008; Graf et al., 2008; Selesnick et al., 2013). In addition, the energy of enhanced drift-loss cone electron fluxes presents an L-shell dependence which is consistent with the first-order cyclotron resonance energy due to VLF transmitter waves, suggesting the important role of VLF transmitters in electron losses (Gamble et al., 2008; Sauvaud et al., 2008). A recent study of Claudepierre et al. (2020b) reported bifurcated inner electron belt with a local minimum in the flux radial profile over L = 2 - 3 from August 2016 to February 2017 based on the raw electron flux measurements from the MagEIS (Blake et al., 2013) onboard Van Allen Probes (Mauk et al., 2013), which is energy dependent and consistent with the location where VLF transmitters can theoretically cause efficient scattering effects (Claudepierre et al., 2020b; Ross et al., 2019). The study of Hua et al. (2020) further provided direct quantitative evidence by a case study that VLF transmitters are primarily responsible for bifurcating the energetic electron belt at tens of keV by comparing the results from Van Allen Probes observations and Fokker-Planck diffusion simulations, while other waves including plasmaspheric hiss and lightning-generated whistlers cannot cause bifurcation but can contribute to electron flux decay at higher energies.

Although both studies of Claudepierre et al. (2020b) and Hua et al. (2020) have analyzed inner belt bifurcation based on either about half-a-year Van Allen Probes MagEIS measurements or a detailed case analysis, there still lacks a systematical analysis to evaluate the statistical distributions of inner energetic electron belt bifurcation, especially using the long-term Van Allen Probes RBSPICE data, the energy coverage of which is suitable for the investigation. Although the wave-induced electron scattering effect is well described by the quasi-linear theory (e.g., Abel et al., 1998a, 1998b; Ross et al., 2019), it is important to investigate the evidence and statistical significance of electron flux decay driven by VLF transmitter waves based on direct in-situ particle measurements. In this letter, the statistical distributions of inner belt bifurcation are provided based on 6-year electron flux measurements from Radiation Belt Storm Probes Ion Composition Experiment (RBSPICE) (Mitchell et al., 2013) onboard Van Allen Probes. Our statistical analysis reveals the potential relation between the inner electron belt bifurcation and VLF transmitter waves, suggesting the roles of VLF transmitter waves in electron losses in the near-Earth space.

2. Observation of Inner Electron Belt Bifurcation

2.1. Van Allen Probes Data

The twin Van Allen probes were launched into near-equatorial orbits with a perigee of \sim 1.1 R_E and an apogee of \sim 5.9 R_E on 30 August 2012 (Mauk et al., 2013). We adopt the Level 3 Pitch Angle and Pressure data set of the RBSPICE, which measures electrons over the energy range from ~25 keV to ~1 MeV with fine energy resolution (Mitchell et al., 2013) to acquire the electron fluxes. The RBSPICE instrument provides 26 energy channels over ~25 - ~118 keV, which is the energy range that we focus on. The present statistics is based on the electron flux at 90° pitch angle measurements during 2013 – 2018 within ±10° of the geomagnetic equator over L = 1 - 3, corresponding to the region where the majority of the wave power of the VLF transmitters is observed (Ma et al., 2017; Meredith et al., 2019). The electron flux data are binned into grids of 0.1 $L \times 1$ day. We adopt the McIlwain L-shell calculated using TS04D magnetic field model (Tsyganenko and Sitnov, 2005). The MagEIS instrument observed the bifurcation feature similar to RBSPICE but with fewer energy channels. The high-resolution (1 minute) OMNIWeb data of geomagnetic indices provided the measurements of SYM-H index,

and AE index with time resolution of 1 minute from the Time History of Events and Macroscale Interaction during Substorms (THEMIS) (Angelopoulos, 2008) is adopted.

125

126

2.2. Identification Criteria of Bifurcated Inner Electron Belt

- 127 An overview of the electron flux evolutions at L = 1.2 - 3.0 and identifications of the bifurcated inner belt during 2016 are presented in Figure 1. Several geomagnetic storms and 128 129 substorms are observed as indicated by the SYM-H and AE indices (Figure 1a-1b). Figures 1c-f 130 display daily-averaged electron fluxes from ~ 30 to ~ 100 keV as a function of L-shell and time. 131 Several events of bifurcated electron belt are observed following electron flux enhancements 132 with the most significant flux decay at $L = \sim 2.3$. Distinct from the one-peak inner belt shown in 133 Figure 1j, Figure 1i shows one example of inner energetic electron belt bifurcation during a 17-134 day period. The inner belt gradually evolves from a one-peak structure following the 135 disturbances on 20 February 2016 to a clear double-peak structure during the quiet period, until the arrival of next electron injection on 07 March 2016. Based on the daily-averaged electron 136 137 flux data with the resolution of 0.1 $L \times 1$ day, the inner electron belt bifurcation can be 138 automatically identified using the following criteria:
- 1. The radial profile of electron flux has at least one local flux minimum (or flux dip) in the inner belt at $L \le 2.4$.
- 2. Since the electron loss timescales due to the VLF transmitters are at least several days as the intensities of VLF transmitter waves are relatively weak (e.g., Ross et al., 2019), the flux ratio of the local flux minimum (j_{min}) to local flux maximum should be smaller than one but not too small as the flux dip is not expected to be too sharp. Here we define the $ratio1 = \frac{j_{min}}{j_{max1}}$ and $ratio2 = \frac{j_{min}}{j_{max2}}$, where j_{max1} and j_{max2} represent local flux maxima peak at L-shells below and above the flux dip, respectively. Therefore, we set the threshold as 0.75 <
- 147 $ratio1 \le 0.98 \text{ and } 0.75 < ratio2 \le 0.98.$
- 3. Significant injections due to the impacts of interplanetary shock on the Earth's magnetosphere (e.g., Li et al., 1993) and enhanced convection electric fields (e.g. Su et al., 2016), and inward radial diffusion driven by ultra-low-frequency waves (e.g., Hua et al., 2019; Li & Hudson, 2019; Lyons & Thorne, 1973) can cause electron flux enhancements, which can penetrate down to the inner belt and easily compromise the bifurcation to one-

- peak inner belt. Therefore, we exclude days of measurements when geomagnetic conditions are very active, i.e., AE > 900 nT or SYM-H < -50 nT.
- 155 4. To avoid injections, we also exclude data if there are flux enhancements compared to the flux level in the past three days, which is defined by $\frac{j(t)}{j(t-i)} > 1.2$, where *t* represents selected days and *i* is selected from 1 to 3 days.

159

160

161

162

163

164

165

166

167

168

169

170

171

172

173

174

175

176

177

178

179

180

181

182

183

5. During the injections or inward radial diffusions, electron fluxes can be enhanced firstly at outer boundary of the inner belt (e.g. Su et al., 2016), leading to a second flux local maximum at L-shells close to \sim 3.0 apart from the original flux peak in the inner belt before the electrons are transported down to the center of the inner belt. To distinguish this double-peak structure from the bifurcated inner electron belt driven by VLF transmitters, we exclude data where $f_{avg}(2.5:2.7) < f_{avg}(2.8:3.0)$, where $f_{avg}(a:b)$ is the averaged flux of electrons at L-shells between a and b.

Distinct from one-peak inner belt, the double-peak bifurcated inner electron belts are automatically identified indicated by the black plus signs in Figures 1c-f, which represents the local flux minimum of the identified bifurcation dip. The identification of bifurcation during other years is presented in Figures S1-S5 of the Supporting Information. Typically, the bifurcation can last for several days under non-disturbed conditions before interrupted by injections or radial diffusion that penetrated down to inner belt, and then the inner belt is transformed into a one-peak structure. Most bifurcation events were observed during nondisturbed periods several days after significant flux enhancement with strong AE index (> 1200 nT, see Table S1 in Supporting Information), which overall elevates the electron fluxes at L >~2.0 so that the flux radial profile distributions become flat, providing the favorable electron flux pre-condition for the formation of the bifurcation (e.g., Figure 1i). However, not all flux enhancements followed by a relatively long quiet time period show inner electron belt bifurcation (e.g., Figure 1j). Besides, the electron flux enhancements occurred too frequently during August 2016, without a subsequent long non-disturbed period for electron flux decay, making it difficult to form the bifurcation. Therefore, the formation of the bifurcation requires relatively quiet geomagnetic conditions, so that other processes such as electron accelerations due to magnetosonic waves or injections will not interrupt the electron loss due to pitch-angle scattering by VLF transmitter waves, aided by plasmaspheric hiss and lightning-generated whistlers. Figure 1g shows the L-shells of the identified bifurcation dip, i.e., local flux minimum

at L < 3.0 as a function of electron energy and time, which can be frequently observed for electrons at $25 - \sim 120$ keV, demonstrating a clear trend that L-shells of the bifurcation dip decrease with increasing energies. Figure 1h indicates the flux ratio, which is the smaller one of aforementioned ratio1 and ratio2. Overall, the flux ratio is above ~ 0.8 , which agrees with previous studies that the electron loss due to VLF scattering effects is a relatively slow process (Claudepierre et al. 2020b; Hua et al., 2020; Ross et al., 2019).

2.3. Electron Flux Pre-condition Selection for Inner Electron Belt Bifurcation

We also automatically selected the electron flux pre-condition for the formation of inner belt bifurcation, by identifying the flux enhancements that penetrate down to the inner belt based on the daily-averaged 90° pitch-angle fluxes. We identified the flux enhancement by comparing to the flux level in the past three days, which is defined by $\frac{j(t)}{j(t-i)} > 1.2$, where t represents selected days and i is selected from 1 to 3 days. The commencement of the enhancement is selected if this flux enhancement occurred for at least 10 L-shell bins and at least 10 energy channels for low electrons (energies below 200 keV), where the L-shell grid is from 1.0 to 3.0 with step of 0.1. To avoid overlapping events of enhancement, we excluded cases in which two individual enhancements occurred within ±3 days of each other. After selecting all the electron flux enhancements in the inner belt, we further identify the electron flux pre-condition for the bifurcation. In order to exclude the scattered and discontinuous identified bifurcation, we only include data where bifurcation occurs for at least 5 days and in more than 10 energy channels during one enhancement event, which we denoted as a bifurcation event. There are more than 20 bifurcation events, with the clear ones listed in Table S1 of the Supporting Information. The first day of the observed bifurcation at any energy channel is defined as the start of the bifurcation event. The electron flux pre-condition is chosen as the flux profile one day before the start of the bifurcation event.

208209

210

211

212

213

184

185

186

187

188

189

190

191

192

193

194

195

196

197

198

199

200

201

202

203

204

205

206

207

3. Statistical Results of Inner Electron Belt Bifurcation

3.1 Electron Flux Pre-condition Features and Dependence on Geomagnetic Activity

As discussed above, not all flux enhancements with a following quiet time period were followed by inner electron belt bifurcation. To quantitively analyze the favorable electron flux pre-condition for the bifurcation, Figures 2a-d present identified pre-condition for the bifurcation

during 2013 – 2018 at the indicated electron energies of 31.0 – 104.9 keV, and the mean profile (red curves). The shaded regions represent the *L*-shell range of electron flux decrease within 10% from the peak of the mean profiles, with the width of the shaded regions (ΔL) marked below. For comparison, we investigate the electron flux distributions which are not followed by bifurcation, by showing the corresponding flux profiles at the commencement of flux enhancements, i.e., the day of the start of the flux enhancement, under relatively quiet geomagnetic conditions (SYM-H > -50 nT) in Figures 2e-h. Clearly, the electron flux pre-conditions of the flux radial profile for bifurcation (Figures 2a-d) are flatter at $L = \sim 2.0 - \sim 2.6$ with most $\Delta L > \sim 1.0$, while it is less likely to form a second peak at L > 2.0 with initial flux radial profiles peaking sharply at $L < \sim 2.0$ ($\Delta L < \sim 0.7$, Figures 2e-h). Besides, the pitch-angle scattering of electrons at energies of tens of keV due to VLF transmitter waves is most efficient at $L > \sim 2.2$ (Hua et al., 2020). This comparison suggests that the formation of inner belt bifurcation more likely occurs on a relatively flat radial profile of enhanced electron fluxes due to injections or radial diffusion.

The occurrence of bifurcated inner electron belt depends significantly on the geomagnetic activity due to the association with injections and radial diffusion. Figure 2i presents the occurrence rate of bifurcation during non-disturbed time as a function of year at color-coded energies with the magenta dashed line showing the yearly-averaged AE index. The counts of the identified bifurcation are shown in Figure 2j. One count means that a bifurcation is identified based on daily-averaged electron fluxes measured by RBSPICE onboard both Van Allen Probes. The yearly-averaged AE index peaks at year 2015 indicating more electron flux injections that can potentially elevate inner belt electron fluxes providing electron flux pre-condition for the bifurcation. However, the occurrence rate of the bifurcation in 2015 is overall lower than that in 2016, as the gradual formations of inner belt bifurcation are interrupted by the frequent injections in 2015. The occurrence rate of the bifurcation is overall higher during 2016 – 2017 than other years, mainly due to the higher AE level during 2016 – 2017 than 2013 – 2014, and 2018, which potentially provides more favorable electron flux pre-conditions for the bifurcation, while there are sufficient non-disturbed periods subsequent to the flux enhancements, allowing electron flux decay due to VLF transmitter waves.

3.2 Dependence on Electron Energy

The statistical distributions of the L-shells of the bifurcation dip as a function of electron energy during 2013 - 2018 are shown in Figure 3a. Here one data count means that bifurcated

inner electron belt is identified based on daily-averaged electron fluxes measured by RBSPICE onboard both Van Allen Probes. Bifurcation is observed at energies over 25 - ~120 keV with bifurcation dips over L = 1.7 - 2.4. Clearly, more cases of bifurcation are observed at energies of $\sim 30 - 80$ keV with bifurcation dips at L = 2.1 - 2.2, and the number of counts decreases significantly above ~ 100 keV. The mean L-shell profile of the bifurcation dips (shown as black line with plus sign) decreases with increasing energy, which is roughly consistent with the firstorder cyclotron resonance energies (indicated by the magenta dashed line) of electrons interacting with 24 kHz VLF transmitter waves at the geomagnetic equator, calculated using the dipole magnetic field model and the empirical plasmaspheric density model by Ozhogin et al. (2012). Besides, the L-shells of bifurcation dip are mostly found at $L > \sim 2.0$, which indicates that the bifurcation can possibly be driven by VLF transmitters located at $L \ge \sim 2$. Although the wave power from the transmitters located at $L < \sim 2$, such as NWC transmitter, can extend to higher Lshells, their wave intensity decreases for more than one order away from the location of the transmitter (Meredith et al., 2019). At L > 2, the wave intensity due to the spread out of the transmitter waves from NWC is lower than the wave intensity originating from the transmitters at L > 2. The transmitters located at $L < \sim 2$ may play a minor role in bifurcation as their wave power is mostly confined within $L = \sim 2$. The majority of the VLF wave power at $L > \sim 2$ comes from DHO38 transmitter (23.4 kHz, L = 2.38, 300 kW) located in Germany, and the NAA transmitter (24.0 kHz, L = 2.74, 1000 kW) and the NLK transmitter (24.8 kHz, L = 2.88, 250 kW) located in North America (e.g., Meredith et al., 2019), which potentially play a major role in driving bifurcation. The yearly results during 2013 - 2018 are shown in Figures 3b-g, respectively, demonstrating similar energy dependence, i.e., the L-shell of the bifurcation dip decreases with increasing energy and approximately follows the first-order cyclotron resonance energies of electrons due to VLF transmitter waves. Besides, consistent with the results discussed above, the counts of the bifurcation are much higher during 2016 – 2017 than in other years.

3.3 Dependence on Season

245

246

247

248

249

250

251

252

253

254

255

256

257

258

259

260

261

262

263

264

265

266

267

268

269

270

271

272

273

274

275

Figures 4a-4b show the occurrence rate and data count of the inner electron belt bifurcation as a function of electron energy for all seasons (black), Northern Hemisphere summer (April – October, in blue) and winter (November – March, in red) under non-disturbed geomagnetic conditions (i.e., AE < 900 nT and SYM-H > -50 nT) during 2013 – 2018. Based on

6-year statistics, the bifurcation is more likely to occur for 30 - 100 keV electrons with the occurrence rate of ~15% during all seasons (black), while the occurrence rate drops significantly down to <10% at energies of ~120 keV. Interestingly, the occurrence rate of the bifurcation depends significantly on season, which is higher during winter than summer with the highest occurrence rate above 20% for ~40 – ~60 keV electrons. This seasonal asymmetry is consistent with previous statistics that the wave intensity of the VLF transmitters is stronger during local winter at L > 1.7 where the wave power mainly comes from the North American transmitters NAA and NLK and German transmitter DHO38 (Meredith et al., 2019), resulting from the lower electron density in the reduced sunlight leading to the decrease of transionospheric wave attenuation (Helliwell, 1965). The yearly results during 2013 - 2018 are shown in Figures 4c-n, respectively, showing similar seasonal dependence of the occurrence rate, which is overall higher during northern hemisphere winter than summer. Furthermore, the occurrence rate of the bifurcation is much higher in 2016 than in other years, which reaches ~50% for ~40 keV electrons and maintains >40% for ~30 - ~80 keV electrons, while the occurrence rate is extremely low during 2013 - 2014.

4. Conclusions and Discussions

In the present study, the statistical distributions of inner electron belt bifurcation are investigated based on 6-year near-equatorial electron flux measurements by RBSPICE onboard both Van Allen Probes during 2013 - 2018. Overall, the bifurcated inner electron belt can be identified based on our data selection criteria. It is noteworthy that there are still some uncertainties about the selection of the threshold of each parameter, such as the *L*-shell of the bifurcation dip (criterion 1) and the flux ratio (ratio1 and ratio2 in criterion 2). To check the sensitivity on these assumptions, we also tried to use the $L \le 2.5$ for the first criteria, which only gives few more counts for the identified bifurcation with a bifurcation dip at L = 2.5. We also tried to set the upper limit of ratio1 and ratio2 as 0.95, the results of which show similar trend but with ~40% counts less than the current results. After trying different upper limits of ratio1 and ratio2 from 0.95 – 0.98, we selected the upper limit as 0.98 which shows the best accuracy of identification of bifurcation. The lower limit ratio of 0.75 in the second criterion can help to avoid false identifications of bifurcation at energies > 130 keV, which are mostly caused by injections. Furthermore, the statistical results without criterion 4 overall still demonstrate similar

- 307 results except for identifying a few more sparse bifurcations, which are mostly caused by
- 308 injections. Besides, the inner energetic electron bifurcation can possibly exist at energies below
- 309 ∼25 keV, which is not included in our study.
- 310 Our principle conclusions are as follows:
- 311 1. The bifurcated inner electron belt can be frequently observed at $\sim 30 100$ keV with
- bifurcation dips at $L > \sim 2.0$ under non-disturbed geomagnetic conditions after significant flux
- enhancements, which can elevate electron fluxes at L = 2.0 2.5 and produce a relatively
- flat electron flux radial profile as the favorable electron flux pre-condition for the bifurcation
- formation. The bifurcation can typically last for a few days from ~5 to ~13 days before
- interrupted by flux enhancements driven by injections or radial diffusion, and then evolve to
- 317 the one-peak inner belt structure.
- 318 2. The L-shell of the bifurcation dip is energy dependent, decreasing with increasing energy,
- which is roughly consistent with the cyclotron resonant energies of electrons due to VLF
- transmitter signals.
- 321 3. The occurrence rate of the bifurcation is higher during local winter than summer, which is
- consistent with the stronger wave intensity of the VLF transmitter waves during local winter
- at L > 1.7 where the wave power mainly comes from the North American transmitters NAA
- and NLK and German transmitter DHO38 (Ma et al., 2017; Meredith et al., 2019).
- 325 4. The L-shell distribution of the bifurcation dip, energy and seasonal dependences of the
- occurrence of bifurcated inner electron belt support the important role of VLF transmitter
- signals in electron flux decay in the inner belt in addition to other naturally occurring waves
- 328 (Hua et al., 2020). The present statistics is therefore crucial to understand when and where
- the VLF transmitters can efficiently scatter energetic electrons (at tens of keV) in near-Earth
- space.
- Our study reveals the location preference and occurrence pattern of the inner belt bifurcation and
- its dependences on geomagnetic condition, season, and pre-condition of electron fluxes. Despite
- 333 the generally weak amplitude of VLF transmitter waves, the electron flux survey indicates the
- deformation of inner radiation belt due to VLF transmitter signals, the effect of which is evident
- especially during geomagnetically quiet periods.

- We acknowledge the Van Allen Probes mission, particularly the RBSPICE team for providing
- 339 the particle data. The RBSPICE data were obtained from http://rbspicea.ftecs.com. We also
- 340 thank the NSSDC OMNIWeb for the use of SYM-H index
- 341 (https://omniweb.gsfc.nasa.gov/ow.html) and the THEMIS mission for providing the AE index
- 342 (http://themis.ssl.berkeley.edu/data/themis/thg/l1/mag/idx/). This work was supported by the
- 343 NSFC grants 42025404, 41904144, 41674163, and 41704162, the B-type Strategic Priority
- Program of the Chinese Academy of Sciences (Grant No. XDB41000000), the pre-research
- projects on Civil Aerospace Technologies No. D020308, D020104, and D020303 funded by the
- 346 China National Space Administration, China Postdoctoral Science Foundation (2020M672405),
- and the National Postdoctoral Program for Innovative Talents (BX20190252). WL would like to
- acknowledge the NSF grants of AGS-1723588 and AGS-1847818, and the Alfred P. Sloan
- Research Fellowship FG-2018-10936.

351 References

- Abel, B., & Thorne, R. M. (1998a). Electron scattering loss in Earth's inner magnetosphere: 1.
- Dominant physical processes. Journal of Geophysical Research: Space Physics, 103(A2),
- 354 2385-2396. https://doi.org/10.1029/97JA02919
- Abel, B., & Thorne, R. M. (1998b). Electron scattering loss in Earth's inner magnetosphere: 2.
- Sensitivity to model parameters. Journal of Geophysical Research: Space Physics, 103(A2),
- 357 2397-2407. https://doi.org/10.1029/97JA02920
- Albert, J. M., Starks, M. J., Horne, R. B., Meredith, N. P., & Glauert, S. A. (2016). Quasi-linear
- simulations of inner radiation belt electron pitch angle and energy distributions.
- Geophysical Research Letters, 43(6), 2381-2388. https://doi.org/10.1002/2016GL067938
- 361 Angelopoulos, V. (2008), The THEMIS Mission, Space Science Reviews, 141, 534,
- 362 doi:10.1007/s11214-008-9336-1.
- 363 Baker, D. N., Kanekal, S. G., Li, X., Monk, S. P., Goldstein, J., & Burch, J. L. (2004). An
- extreme distortion of the Van Allen belt arising from the 'Hallowe'en'solar storm in 2003.
- Nature, 432(7019), 878. https://doi.org/10.1038/nature03116
- Baker, D. N., Kanekal, S. G., Horne, R. B., Meredith, N. P., & Glauert, S. A. (2007). Low-
- altitude measurements of 2–6 MeV electron trapping lifetimes at $1.5 \le L \le 2.5$. Geophysical
- Research Letters, 34(20). https://doi.org/10.1029/2007GL031007

- Baker, D. N., & Blake, J. B. (2012). SAMPEX: A long-serving radiation belt sentinel. Dynamics
- of the Earth's Radiation Belts and Inner Magnetosphere, 21-40.
- 371 https://doi.org/10.1029/2012GM001368
- Blake, J. B., Carranza, P. A., Claudepierre, S. G., Clemmons, J. H., Crain, W. R., Dotan, Y., et al.
- 373 (2013). The magnetic electron ion spectrometer (MagEIS) instruments aboard the radiation
- belt storm probes (RBSP) spacecraft. Space Science Reviews, 179(1-4), 383–421.
- 375 https://doi.org/10.1007/s11214-013-9991-8
- Cao, X., Ni, B., Summers, D., Zou, Z., Fu, S., & Zhang, W. (2017). Bounce resonance scattering
- of radiation belt electrons by low-frequency hiss: Comparison with cyclotron and Landau
- 378 resonances. Geophysical Research Letters, 44, 9547–9554.
- 379 https://doi.org/10.1002/2017GL075104
- Cao, X., Ni, B., Summers, D., Fu, S., & Shi, R. (2020). Hot plasma effects on the pitch-angle
- scattering rates of radiation belt electrons due to plasmaspheric hiss. The Astrophysical
- Journal, 896(2), 118. http://dx.doi.org/10.3847/1538-4357/ab9107
- 383 Chen, Y.P., Yang, G.B., Ni, B.B., Zhao, Z.Y., Gu, X.D., Zhou, C., & Wang, F. (2016).
- Development of ground-based ELF/VLF receiver system in Wuhan and its first results.
- 385 Advances in Space Research, 57(9), 1871-1880. https://doi.org/10.1016/j.asr.2016.01.023.
- 386 Chen Y, Ni B, Gu X, et al. (2017). First observations of low latitude whistlers using WHU
- 387 ELF/VLF receiver system. Science China-technological Sciences, 60(1): 166-174.
- Claudepierre, S. G., O'Brien, T. P., Looper, M. D., Blake, J. B., Fennell, J. F., Roeder, J. L., ... &
- Spence, H. E. (2019). A revised look at relativistic electrons in the Earth's inner radiation
- zone and slot region. Journal of Geophysical Research: Space Physics, 124(2), 934-951.
- 391 https://doi.org/10.1029/2018JA026349
- Claudepierre, S. G., Ma, Q., Bortnik, J., O'Brien, T. P., Fennell, J. F., & Blake, J. B. (2020a).
- Empirically estimated electron lifetimes in the Earth's radiation belts: Van Allen Probe
- 394 observations. Geophysical Research Letters, 47, e2019GL086053.
- 395 https://doi.org/10.1029/2019GL086053
- Claudepierre, S. G., Ma, Q., Bortnik, J., O'Brien, T. P., Fennell, J. F., & Blake, J. B. (2020b).
- Empirically estimated electron lifetimes in the Earth's radiation belts: Comparison with
- theory. Geophysical Research Letters, 47, e2019GL086056.
- 399 https://doi.org/10.1029/2019GL086056

- Clilverd, M. A., Rodger, C. J., Gamble, R., Meredith, N. P., Parrot, M., Berthelier, J. J., &
- Thomson, N. R. (2008). Ground-based transmitter signals observed from space: Ducted or
- 402 nonducted? Journal of Geophysical Research: Space Physics, 113(A4).
- 403 https://doi.org/10.1029/2007JA012602
- Gamble, R. J., Rodger, C. J., Clilverd, M. A., Sauvaud, J.-A., Thomson, N. R., Stewart, S. L.,
- 405 McCormick, R. J., Parrot, M., and Berthelier, J.-J. (2008), Radiation belt electron
- precipitation by man-made VLF transmissions, Journal of Geophysical Research: Space
- 407 Physics, 113, A10211. https://doi.org/10.1029/2008JA013369
- 408 Graf, K. L., Inan, U. S., Piddyachiy, D., Kulkarni, P., Parrot, M., and Sauvaud, J. A. (2009),
- DEMETER observations of transmitter-induced precipitation of inner radiation belt
- 410 electrons, Journal of Geophysical Research, 114, A07205.
- 411 https://doi.org/10.1029/2008JA013949
- Green, A., Li, W., Ma, Q., Shen, X.-C., Bortnik, J., & Hospodarsky, G. B. (2020). Properties of
- lightning generated whistlers based on Van Allen Probes observations and their global
- effects on radiation belt electron loss. Geophysical Research Letters, 47, e2020GL089584.
- 415 <u>https://doi.org/10.1029/2020GL089584</u>
- 416 Gu, X., Xia, S., Fu, S., Xiang, Z., Ni, B., Guo, J., & Cao, X. (2020). Dynamic responses of
- radiation belt electron fluxes to magnetic storms and their correlations with magnetospheric
- plasma wave activities. The Astrophysical Journal, 891(2), 127 (11pp).
- 419 https://doi.org/10.3847/1538-4357/ab71fc
- 420 Helliwell, R. A. (1965), Whistlers and Related Ionospheric Phenomena, pp. 288–316, Stanford
- 421 Univ. Press, Stanford, Calif.
- 422 Hua, M., Li, W., Ma, Q., Ni, B., Nishimura, Y., Shen, X.-C., & Li, H. (2019). Modeling the
- electron flux enhancement and butterfly pitch angle distributions on L shells <2.5.
- 424 Geophysical Research Letters, 46, 10967–10976. https://doi.org/10.1029/2019GL084822
- 425 Hua, M., Li, W., Ni, B., Ma, Q., Green, A., Shen, X.-C., ... & Reeves, G. D. (2020). Very-Low-
- Frequency transmitters bifurcate energetic electron belt in near-earth space. Nature
- 427 Communications, 11, 4847. https://doi.org/10.1038/s41467-020-18545-y
- 428 Li, W., & Hudson, M. K. (2019). Earth's Van Allen radiation belts: From discovery to the Van
- 429 Allen Probes era. Journal of Geophysical Research: Space Physics, 124, 8319–8351.
- 430 https://doi.org/10.1029/2018JA025940

- Li, X., Roth, I., Temerin, M., Wygant, J. R., Hudson, M. K., & Blake, J. B. (1993). Simulation of
- the prompt energization and transport of radiation belt particles during the March 24, 1991
- 433 SSC. Geophysical Research Letters, 20(22), 2423-2426. https://doi.org/10.1029/93GL02701
- 434 Lyons, L. R., & Thorne, R. M. (1973). Equilibrium structure of radiation belt electrons. Journal
- of Geophysical Research, 78(13), 2142-2149. https://doi.org/10.1029/JA078i013p02142
- 436 Ma, Q., et al. (2016), Characteristic energy range of electron scattering due to plasmaspheric hiss,
- 437 J. Geophys. Res. Space Physics, 121, 11,737–11,749, doi:10.1002/2016JA023311.
- 438 Ma, Q., Mourenas, D., Li, W., Artemyev, A., & Thorne, R. M. (2017). VLF transmitters from
- ground-based transmitters observed by the Van Allen Probes: Statistical model and effects
- on plasmaspheric electrons. Geophysical Research Letters, 44(13), 6483-6491.
- 441 https://doi.org/10.1002/2017GL073885
- 442 Ma, X., Xiang, Z., Ni, B., Fu, S., Cao, X., Hua, M., Guo, D. Y., Guo, Y. J., Gu, X. D., Liu, Z. Y.
- and Zhu, Q. (2020). On the loss mechanisms of radiation belt electron dropouts during the
- 444 12 September 2014 geomagnetic storm. Earth Planet. Phys., 4(6), 598–610, doi:
- 445 10.26464/epp2020060
- 446 Mauk, B. H., Fox, N. J., Kanekal, S. G., Kessel, R. L., Sibeck, D. G., & Ukhorskiy, A. (2013).
- Science objectives and rationale for the Radiation Belt Storm Probes mission. Space
- Science Reviews, 179(1–4), 3–27. https://doi.org/10.1007/s11214-012-9908-y
- Meredith, N. P., Horne, R. B., Glauert, S. A., & Anderson, R. R. (2007). Slot region electron loss
- 450 timescales due to plasmaspheric hiss and lightning-generated whistlers. Journal of
- Geophysical Research: Space Physics, 112(A8). https://doi.org/10.1029/2007JA012413
- 452 Meredith, N. P., Horne, R. B., Clilverd, M. A., & Ross, J. P. (2019). An investigation of VLF
- 453 transmitter wave power in the inner radiation belt and slot region. Journal of Geophysical
- 454 Research: Space Physics, 124(7), 5246-5259. https://doi.org/10.1029/2019JA026716
- 455 Mitchell, D. G., Lanzerotti, L. J., Kim, C. K., Stokes, M., Ho, G., Cooper, S., ... & Brandt, P.
- 456 (2013). Radiation belt storm probes ion composition experiment (RBSPICE). In The Van
- Allen Probes Mission (pp. 263-308). Springer, Boston, MA. https://doi.org/10.1007/978-1-
- 458 4899-7433-4 8
- Ni, B., et al. (2014), Resonant scattering of energetic electrons by unusual low-frequency hiss,
- 460 Geophys. Res. Lett., 41, 1854–1861. https://doi.org/10.1002/2014GL059389

- Ni, B., Huang, H., Zhang, W., Gu, X., Zhao, H., Li, X., et al. (2019). Parametric sensitivity of the
- formation of reversed electron energy spectrum caused by plasmaspheric hiss. Geophysical
- 463 Research Letters, 46, 4134–4143. https://doi.org/10.1029/2019GL082032
- Ozhogin, P., Tu, J., Song, P., & Reinisch, B. W. (2012). Field-aligned distribution of the
- plasmaspheric electron density: An empirical model derived from the IMAGE RPI
- 466 measurements. Journal of Geophysical Research: Space Physics, 117(A6).
- 467 https://doi.org/10.1029/2011JA017330
- Reeves, G. D., Friedel, R. H. W., Larsen, B. A., Skoug, R. M., Funsten, H. O., Claudepierre, S.
- G., ... & Spence, H. E., et al. (2016), Energy-dependent dynamics of keV to MeV electrons
- in the inner zone, outer zone, and slot regions, Journal of Geophysical Research: Space
- 471 Physics, 121, 397–412. https://doi.org/10.1002/2015JA021569
- Rodger, C. J., & Clilverd, M. A. (2002). Inner radiation belt electron lifetimes due to whistler-
- induced electron precipitation (WEP) driven losses. Geophysical research letters, 29(19),
- 474 30-1. https://doi.org/10.1029/2002GL015795
- Rodger, C. J., Clilverd, M. A., & McCormick, R. J. (2003). Significance of lightning-generated
- 476 whistlers to inner radiation belt electron lifetimes. Journal of Geophysical Research: Space
- 477 Physics, 108(A12). https://doi.org/10.1029/2003JA009906
- 478 Rosen, A., & Sanders, N. L. (1971). Loss and replenishment of electrons in the inner radiation
- zone during 1965–1967. Journal of Geophysical Research, 76(1), 110-121.
- 480 https://doi.org/10.1029/JA076i001p00110
- 481 Ross, J. P., Meredith, N. P., Glauert, S. A., Horne, R. B., & Clilverd, M. A. (2019). Effects of
- VLF transmitter waves on the inner belt and slot region. Journal of Geophysical Research:
- 483 Space Physics, 124(7), 5260-5277. https://doi.org/10.1029/2019JA026715
- Sauvaud, J. A., Maggiolo, R., Jacquey, C., Parrot, M., Berthelier, J. J., Gamble, R. J., & Rodger,
- 485 C. J. (2008). Radiation belt electron precipitation due to VLF transmitters: Satellite
- observations. Geophysical Research Letters, 35(9). https://doi.org/10.1029/2008GL033194
- 487 Selesnick, R. S., Albert, J. M., & Starks, M. J. (2013). Influence of a ground-based VLF radio
- 488 transmitter on the inner electron radiation belt. Journal of Geophysical Research: Space
- 489 Physics, 118(2), 628-635. https://doi.org/10.1002/jgra.50095

- 490 Su, Y. J., Selesnick, R. S., & Blake, J. B. (2016). Formation of the inner electron radiation belt
- by enhanced large-scale electric fields. Journal of Geophysical Research: Space
- 492 Physics, 121(9), 8508-8522. https://doi.org/10.1002/2016JA022881
- Tsyganenko, N. A., and Sitnov, M. I. (2005), Modeling the dynamics of the inner magnetosphere
- during strong geomagnetic storms, J. Geophys. Res., 110, A03208,
- 495 doi:10.1029/2004JA010798.
- Walt, M. A. R. T. I. N., & Farley, T. A. (1978). The physical mechanisms of the inner Van Allen
- belt. In: The earth: 1-The upper atmosphere, ionosphere and magnetosphere. (A78-45322
- 498 20-46) New York and London, Gordon and Breach, Science Publishers, 1978, p. 303-412.,
- 499 303-412.
- Xiang, Z., Li, X., Selesnick, R., Temerin, M. A., Ni, B., Zhao, H., et al. (2019). Modeling the
- quasi trapped electron fluxes from cosmic ray albedo neutron decay (CRAND).
- Geophysical Research Letters, 46, 1919–1928. https://doi.org/10.1029/2018GL081730
- 503 Xiang, Z., Li, X., Temerin, M. A., Ni, B., Zhao, H., Zhang, K., & Khoo, L. Y. (2020). On
- energetic electron dynamics during geomagnetic quiet times in Earth's inner radiation belt
- due to atmospheric collisional loss and cosmic ray albedo neutron decay (CRAND) as a
- source. Journal of Geophysical Research: Space Physics, 125, e2019JA027678.
- 507 https://doi.org/10.1029/2019JA027678
- 508 Yi, J., Gu, X. D., Li, Z. P., Lin, R. T., Cai, Y. H., Chen, L., et al. (2019). Modeling and analysis
- of NWC signal propagation amplitude based on LWPC and IRI models. Chinese Journal of
- Geophysics (in Chinese),62(9), 3223-3234.
- Zhang, W., Ni, B., Huang, H., Summers, D., Fu, S., Xiang, Z., et al. (2019). Statistical properties
- of hiss in plasmaspheric plumes and associated scattering losses of radiation belt electrons.
- Geophysical Research Letters, 46, 5670–5680. https://doi.org/10.1029/2018GL081863
- Zhao, H., Ni, B., Li, X. et al. Plasmaspheric hiss waves generate a reversed energy spectrum of
- radiation belt electrons. Nature Physics. 15, 367–372 (2019).
- 516 https://doi.org/10.1038/s41567-018-0391-6

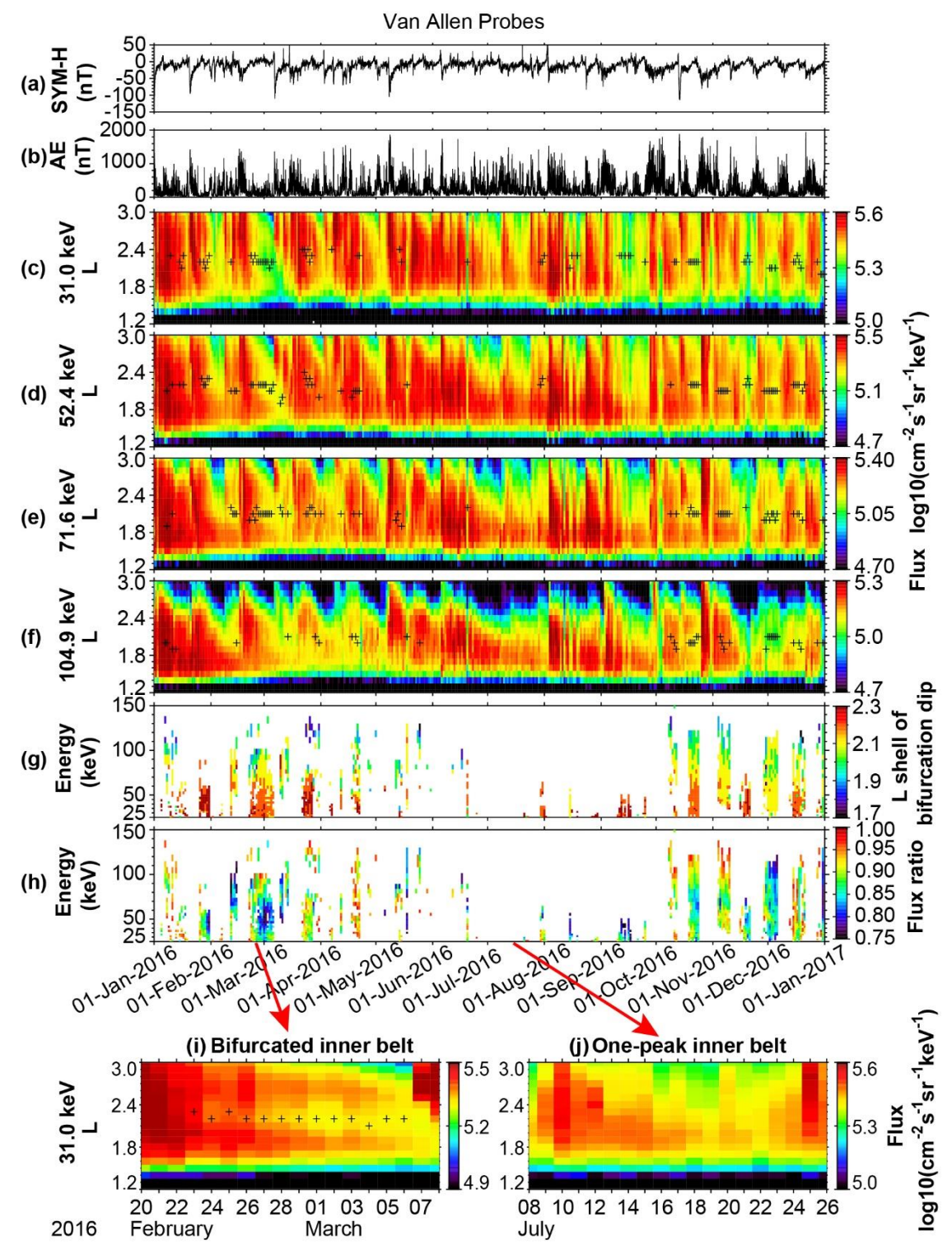


Figure 1. The observation of inner energetic electron belt by Van Allen Probes in year 2016. (a) SYM-H index. (b) AE index. Electron flux evolutions at 90° pitch angle measured by RBSPICE

from both Van Allen Probes within $\pm 10^{\circ}$ of the geomagnetic equator at (c) 31.0, (d) 52.4, (e) 71.6, and (f) 104.9 keV, respectively. The black plus signs represent the local flux minimum of the identified bifurcated inner belt. (g) *L*-shell of the bifurcation dip as a function of energy. (h) Flux ratio of the local flux minimum to the local flux maximum at $L \leq 3.0$. Examples of (i) bifurcated, and (j) one-peak inner belt structures at 31.0 keV in the same format as (c) but during shorter periods.

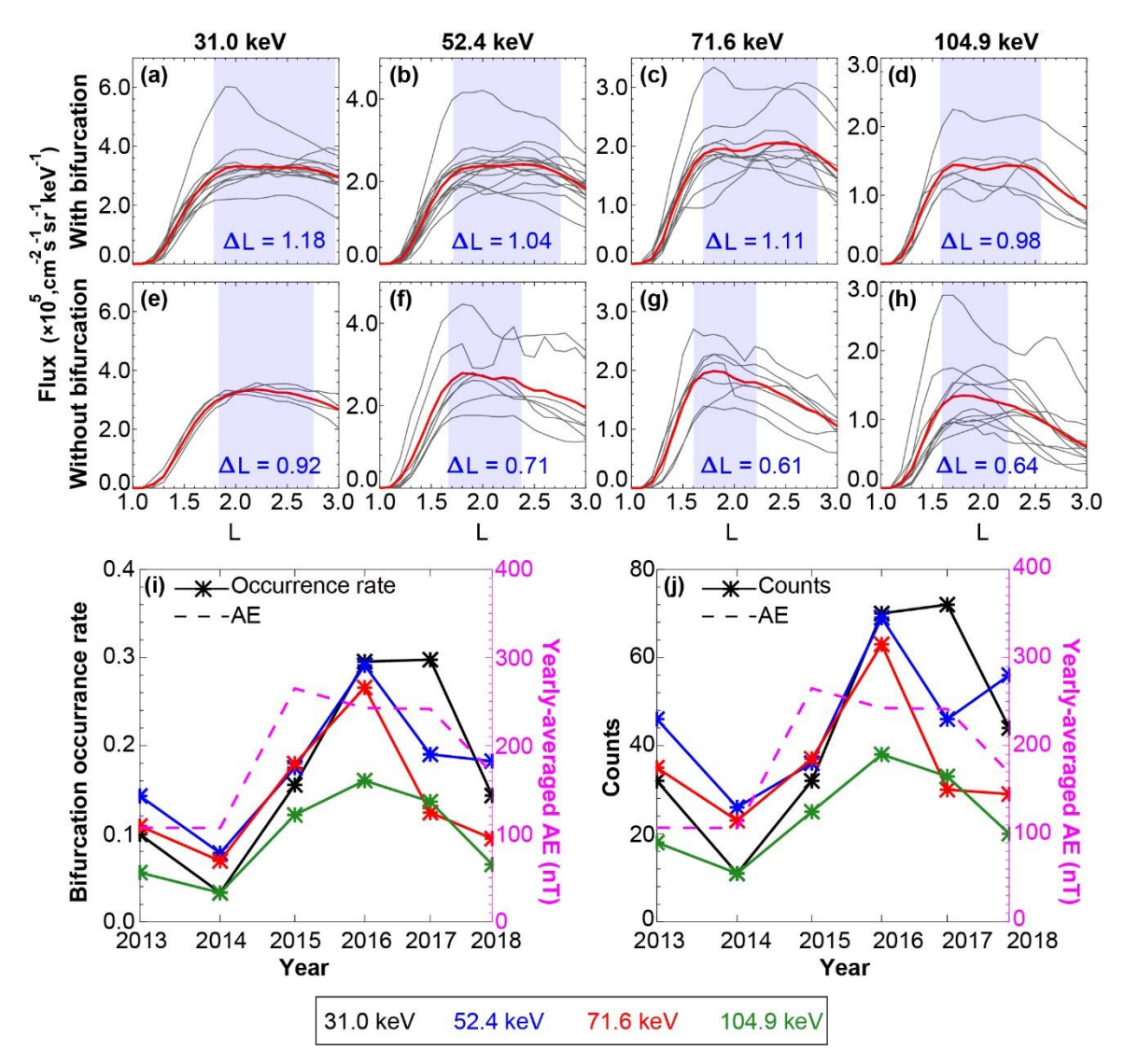


Figure 2. Radial profile of electron fluxes at 90° pitch angle measured by RBSPICE during 2013-2018 after electron flux enhancements that penetrate to the inner belt with (a-d) and without (e-h) subsequent observations of inner belt bifurcation at the indicated electron energies, from left to right: 31.0 keV, 52.4 keV, 71.6 keV, and 104.9 keV, and the mean profile (red curves). The shaded regions represent the electron flux decrease by less than 10% of the flux maximum, with the width of the shaded regions (ΔL) marked below. (i) The occurrence rate of the bifurcated inner belt under non-disturbed geomagnetic conditions (i.e., AE < 900 nT and SYM-H > -50 nT) as a function of year at color-coded electron energies. The magenta dashed line indicates the yearly-averaged AE index. (j) Counts of the identified bifurcated inner belt. One count means that a bifurcated inner belt is identified based on daily-averaged electron fluxes measured by RBSPICE onboard both Van Allen Probes.

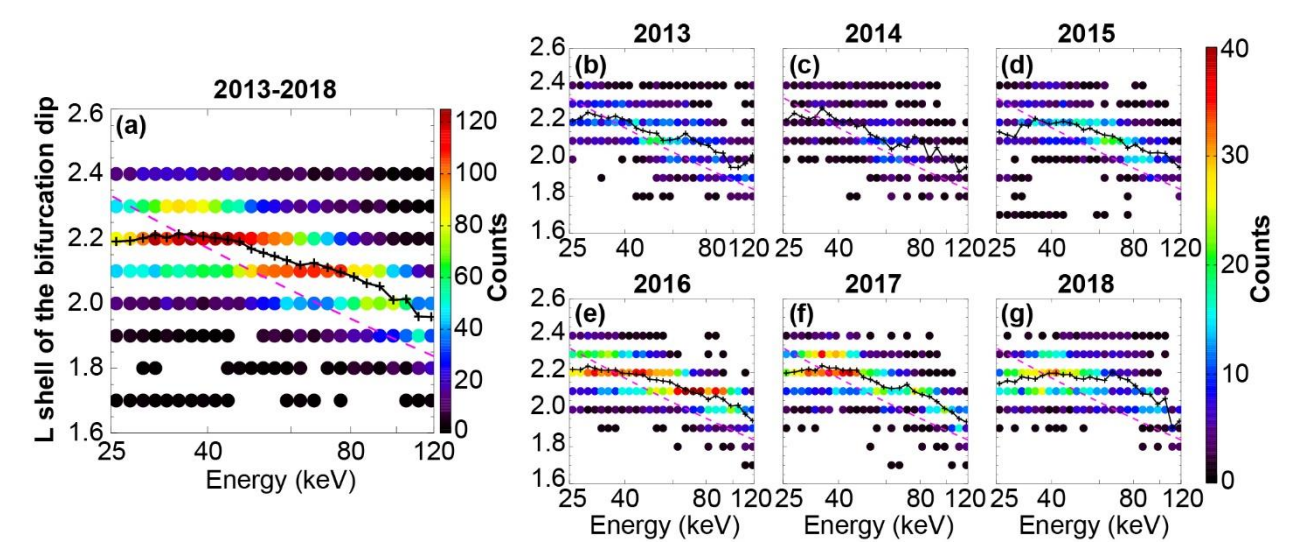


Figure 3. (a) The statistical distribution of the *L*-shell of the bifurcation dip as a function of electron energy during 2013 – 2018. One count means that a bifurcated inner belt is identified based on daily-averaged electron fluxes measured by RBSPICE onboard both Van Allen Probes. The black line with plus sign represents the mean profile. The magenta dashed line indicates the first-order cyclotron resonant energies of electrons interacting with 24 kHz VLF transmitter waves at the geomagnetic equator. (b-g) Same as in (a) except for yearly results from 2013 to 2018.

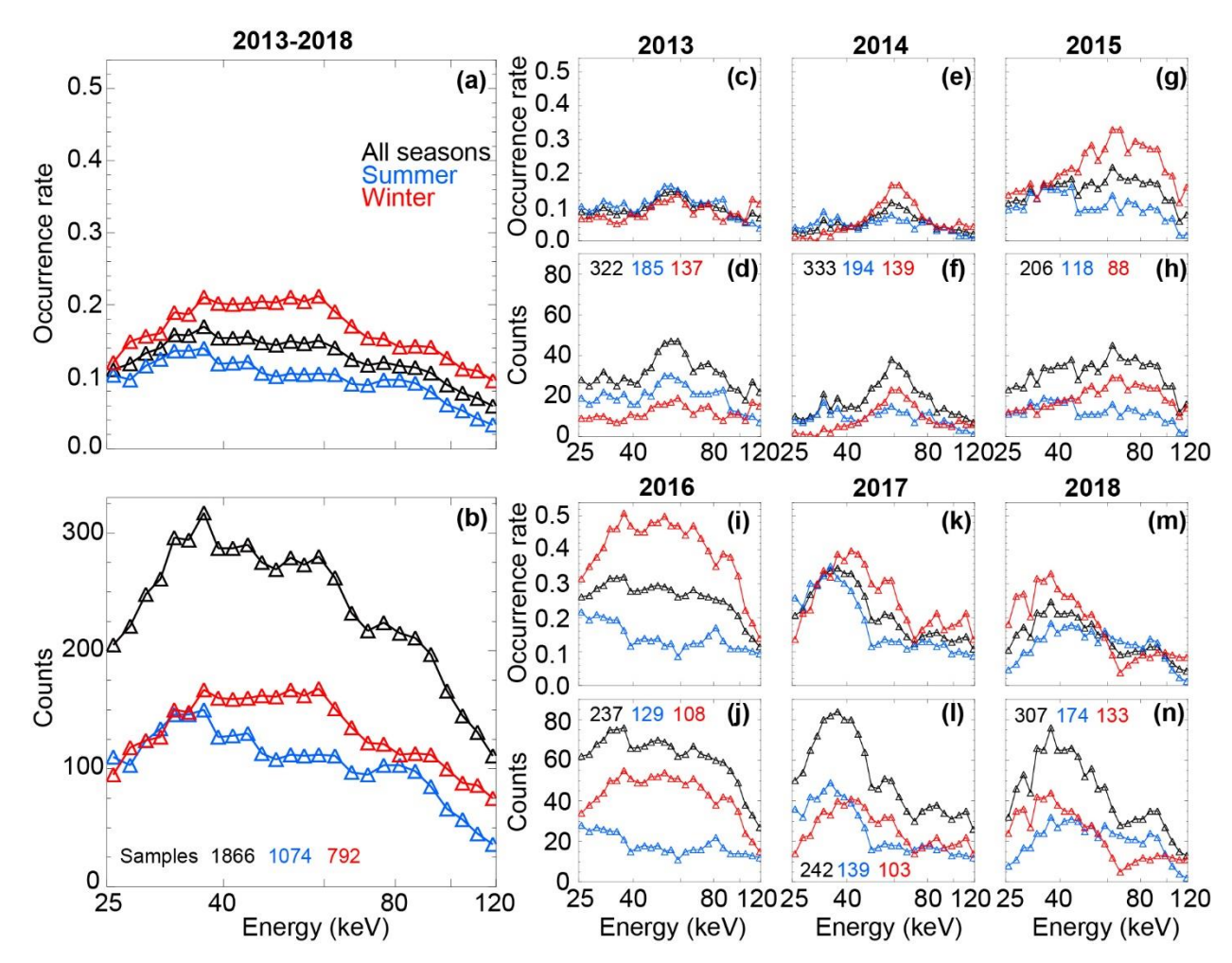


Figure 4. (a) The occurrence rate of the bifurcated inner belt as a function of electron energy for all seasons (black), Northern Hemisphere summer (April – October, in blue) and winter (November – March, in red) under non-disturbed geomagnetic conditions (i.e., AE < 900 nT and SYM-H > -50 nT) during 2013 – 2018. (b) Counts of the identified bifurcated inner belt. One count means that a bifurcated inner belt is identified based on daily-averaged electron fluxes measured by RBSPICE onboard both Van Allen Probes. The sample numbers are marked below, which represent the non-disturbed days during the considered time period. (c-n) Same as in (a-b) except for yearly results.

